

Wavelet balancing for residual moveouts

William S. Harlan¹

ABSTRACT

Conventional moveout analysis stretches and squeezes traces to increase the coherence of reflected amplitudes in prestack seismic gathers. Higher order residual moveouts require increasingly difficult scans of semblances with extra dimensions or picking from correlations with many local minima. Alternatively, we can model our data with an adaptive convolution that assumes consistent reflectivities at all offsets (or angles). Short, convolutional wavelets can adjust residual moveouts arbitrarily with offset, but slowly with time (or depth). A Gauss-Newton optimization easily inverts this transform by minimizing a least-squares objective function. With estimated and normalized wavelets, we deconvolved the original data to remove phase and spectral distortions that affected more than one reflection. By constraining how slowly wavelets adapt, we retained phase and amplitude changes distinctive to individual reflections. Deconvolution also avoided any explicit smoothing or mixing of amplitudes among traces. Estimated wavelets captured residual coherence and were easier to track visually than individually weak reflections. By adjusting the length and number of independent dynamic wavelets, we can adjust the resolution to the redundancy supported by the data.

INTRODUCTION

Much prestack seismic processing requires the adjustment of moveouts — the coherence and phase of reflections over source-receiver offset or reflection angles. Examples are normal moveout (NMO) stretching, surface-consistent static corrections, migration velocity analysis, and even full-waveform inversion. Corrected gathers produce a redundant image of subsurface reflectors, with each trace belonging to a different propagation path. An accurate model

of the kinematics should show consistent coherence across prestack traces.

We use the term *residual moveout* (RMO) for a variety of methods that stretch and squeeze prestack traces to increase their similarity. Such residual corrections do not adjust for amplitudes or phase shifts that vary with frequency.

Conventional NMO analysis is often followed by scans of higher order RMO corrections. These corrections can adjust for anisotropic effects such as earlier arrival times at larger offsets and steeper propagation angles. Moveout curvature can also vary elliptically over source-receiver azimuth due to anisotropic changes in stress and fracturing (Tsvankin and Grechka, 2011). Reference moveouts can be removed before scanning these residual corrections (Adler and Brandwood, 1999; Hu et al., 2013).

Static corrections typically adjust for near-surface distortions that are not easily incorporated in a velocity model. “Second-order statics” or “trim statics” (Cox et al., 1999) is a form of RMO analysis that slowly adjust vertical shifts over the length of a trace to encourage consistency in prestack gathers. This analysis typically relies on crosscorrelations and picking that are vulnerable to cycle-skipping errors (Urnenbach and Bancroft, 2001).

For migration velocity analysis and tomography, RMO analysis is key to iterative updates. In its earliest form (MacKay and Abma, 1993), a constant-offset prestack depth migration is scanned for residual hyperbolic moveouts over offset. Reflection tomography minimizes the variance of migrated depths at different image offsets or angles (Harlan et al., 1991; Stork, 1992).

Full-waveform inversion prefers wave-equation kernels to tomographic raypaths, but still distinguishes reflectivity imaging from low-frequency transmission (Almomin and Biondi, 2013; Lee et al., 2013). Lower frequency updates benefit from RMO analysis such as dynamic image warping, which stretches traces for greater similarity (Hale and Luo, 2013; Hale and Ma, 2013).

Amplitude variation with offset (AVO) interpretation also depends on detecting prestack moveouts accurately. A small RMO creates a large spurious anomaly in a gradient stack (Castagna and Backus, 1993).

Manuscript received by the Editor 30 December 2013; revised manuscript received 3 July 2014; published online 24 October 2014.

¹Halliburton–Landmark, Highlands Ranch, Colorado, USA. E-mail: bill.harlan@gmail.com.

© 2014 Society of Exploration Geophysicists. All rights reserved.

In this paper, we explore how an adaptive convolutional model can address these problems of RMO analysis, with greater control over differences in amplitudes and phase with frequency.

RMO relies on stretching with lags that are a very nonlinear function of trace amplitudes. Local minima prevent any small adjustment of lags from improving the solution. Algorithms depend on nonlinear methods of measuring coherence, such as semblance scans or picking peaks of crosscorrelations.

Convolution, on the other hand, is a linear transform. Wavelet estimation and deconvolution allow least-squares solutions of quadratic objective functions with a single global minimum. Although a convolutional model has more degrees of freedom than an RMO stretch, we can be selective in how we use detected changes in coherence.

A convolutional model can avoid “NMO stretch” by distinguishing time-invariant wavelets from reflections that converge over offset (Lazaratos and Finn, 2004). Unlike static corrections, deconvolution can remove surface-consistent distortions in phase and amplitude (Levin, 1989). Adaptive deconvolution can restore spectral consistency in waves that have propagated for different distances (Griffiths et al., 1977).

The algorithmic formulation is a modification of wavelet balancing (Harlan, 1989), with the addition of dynamic changes over time or depth. We model reflectivities with a single consistent trace that should appear identical at all offsets and angles or vary slowly according to a low-order analytic expression. Residual transmission effects are modeled with a short convolutional wavelet that changes rapidly with offset or angle, but slowly with time or depth. This simple convolutional model can be optimized with a least-squares objective function iteratively solved by a Gauss-Newton algorithm (Luenberger, 1973; Harlan, 2004).

Once we have estimates of wavelets that vary over offset and time (or depth and angle), we can deconvolve the original data and remove residual phase distortions. Appropriate normalization can retain amplitude gradients important to AVO attributes. In our examples, we will preserve the mean-squared energy of the original reflection wavelet but allow for spectral adjustments of amplitude and phase among wavelets. By forcing our dynamic wavelets to vary slowly over a range of reflections, we should also retain phase and amplitude anomalies that are distinctive for any single reflection.

METHODS

We begin with a dynamic variation on the convolutional model of wavelet balancing (Harlan, 1989).

Let us model a single prestack gather $d_j(t)$ of imaged or recorded amplitudes d as a function of depth or time t and of a prestack index j , which might identify various arbitrary offsets, imaged angles, and azimuths. These offsets can be multidimensional and could even include adjacent midpoints in a supergather. We will let t range from 0 to a maximum value of T , and we will index j from 1 to M total traces.

Let us model this gather with a reflectivity $r_j(t)$ that varies slowly with the prestack index j . Residual “transmission” effects are modeled by a time-varying convolutional wavelet $w_j(\tau, t)$. The wavelet amplitude w varies arbitrarily with the prestack index j . The wavelet varies smoothly over the absolute time or depth t and convolves over a short lag τ for a length $\Delta\tau$.

In this way, we can model our data with the convolution

$$d_j(t) = \int_{-\Delta\tau/2}^{\Delta\tau/2} r_j(t - \tau) w_j(\tau, t) d\tau. \quad (1)$$

This equation would appear overdetermined for the reflectivity $r_j(t)$ and wavelet $w_j(\tau, t)$, except for our specifications of smoothness. Reflectivity varies arbitrarily over time t and smoothly over j . The wavelet varies arbitrarily over j and smoothly over time t . In addition, we could remove other degrees of freedom from our wavelets with conditioning or postprocessing.

For example, we can use Shuey’s equation (Shuey, 1985) for a zero-offset reflectivity $r(t)$ and a second-order gradient $g(t)$ that model reflection angles θ_j according to $r_j(t) = r(t) + g(t)\sin^2(\theta_j)$.

For our application and example, we will assume reflectivity does not vary with the prestack index j at all, allowing us to write $r(t)$.

We will model the dynamic wavelet for a single trace j with N time-invariant convolutional wavelets separated at an interval Δt . We will use the index i for these N convolutional wavelets, written as $w_{ij}(\tau)$. Each wavelet will best describe the dynamic convolution at a particular time of $t_i = i\Delta t$. At any intermediate time t , the dynamic wavelet will be a sum of the two nearest convolutional wavelets, with a linear weight summing to one.

We can now write our time-varying dynamic wavelet as

$$w_j(\tau, t) = \sum_{i=1}^N w_{ij}(\tau) \Lambda\left(\frac{t - i\Delta t}{\Delta t}\right). \quad (2)$$

Linear weighting is written with the triangle function $\Lambda(t)$, with an area of one, dropping linearly from a value of one at $t = 0$ to a value of zero at $t = \pm 1$:

$$\Lambda(t) = \begin{cases} 1 - |t| & \text{if } |t| < 1 \\ 0 & \text{if } |t| \geq 1 \end{cases}. \quad (3)$$

We can combine our convolution equation 1 and our dynamic wavelet equation 2 into a single expression for the data as

$$d_j(t) = \int_{-\Delta\tau/2}^{\Delta\tau/2} r(t - \tau) \sum_{i=1}^N \left[w_{ij}(\tau) \Lambda\left(\frac{t - i\Delta t}{\Delta t}\right) \right] d\tau. \quad (4)$$

We also drop trace dependence j from the reflectivity.

Now it should be obvious that our inverse problem is overdetermined. Assume we have $M = 100$ traces of $T = 8$ s each. We need only one reflectivity trace of the same length (or two or three traces to include an AVO gradient). We might chose convolutional wavelets with lag $\Delta\tau$ of 0.1 s and with a dynamic time interval Δt of 1.0 s for $N = 9$. That gives us 800 s of data and only 98 s of unknowns — overdetermined by a factor of eight.

Notice that the forward modeling equation 4 is linear in the wavelet and linear in the reflectivity, but not in both simultaneously. There is nonuniqueness in the scaling of either: we can multiply the reflectivity by a constant and divide the wavelets by the same constant, without altering the result. To resolve this ambiguity, we will assume that the reflectivity has the same amplitude variance as the recorded data, so that it has the amplitude of an averaged stack

trace. We will normalize the wavelets for a root-mean-square (rms) amplitude of one.

Because the convolutional wavelets are relatively short, we may want to discourage a sharp drop in amplitudes at the maximum lag of $\Delta\tau/2$. We could adjust the expected variance of the wavelet at the maximum lag, or we could reparameterize the wavelet equation 2 (Harlan, 1995). For example,

$$w_{ij}(\tau) = \hat{w}_{ij}(\tau) \cdot \cos\left(\frac{\pi\tau}{\Delta\tau}\right), \quad \text{for } -\frac{\Delta\tau}{2} \leq \tau \leq \frac{\Delta\tau}{2}. \quad (5)$$

This tapers a normalized wavelet $\hat{w}_{ij}(\tau)$ with a cosine, from a maximum value of one at zero lag, down to zero at the maximum lag. If our inversion damps the normalized wavelet with a uniform variance, then the resulting convolutional wavelet will decline in expected amplitude with increasing lag.

Substituting equation 5 into equation 4, we get

$$d_j(t) = \int_{-\Delta\tau/2}^{\Delta\tau/2} r(t-\tau) \sum_{i=1}^N \left[\hat{w}_{ij}(\tau) \cdot \cos\left(\frac{\pi\tau}{\Delta\tau}\right) \Lambda\left(\frac{t-i\Delta t}{\Delta t}\right) \right] d\tau. \quad (6)$$

Finally, we can pose our inverse problem with a least-squares objective function. We can write our recorded data traces as $d_j^R(t)$ and minimize

$$\begin{aligned} \min_{r(t), \hat{w}_{ij}(\tau)} J = & \frac{1}{2} \sum_{j=1}^M \int_0^T [d_j(t) - d_j^R(t)]^2 dt \\ & + \frac{\epsilon_w}{2} \sum_{j=1}^M \sum_{i=1}^N \int_{-\Delta\tau/2}^{\Delta\tau/2} \hat{w}_{ij}(\tau)^2 d\tau + \frac{\epsilon_r}{2} \int_0^T r(t)^2 dt. \quad (7) \end{aligned}$$

Here, we minimized the squared error between the recorded data $d_j^R(t)$ and modeled data $d_j(t)$. We also add two damping terms for regularization, to avoid overamplifying poorly resolved components. The small value ϵ_w is the ratio of the expected variance of noise divided by the variance of the wavelet amplitudes. The small value ϵ_r is the variance of noise divided by the variance of the reflectivity. In both cases, we can assume the variance of the unknowns is much larger than the variance of the noise.

We assume the variance of reflectivity to be that of the recorded data amplitudes, and the noise to have 1/1000 of the variance of the reflectivity, so that $\epsilon_r = 0.001$. As mentioned before, wavelets are given an expected variance of one because they multiply the variance of the reflectivity. If data amplitudes are first normalized to one, then $\epsilon_w = 0.001$ also.

Damping has little effect in early iterations of a gradient-based optimization and is only formally necessary for stability after a large number of iterations. (This is one of the advantages of the normalization in equation 5 for waveform variance [Harlan, 1995]). These damping terms have the effect of suppressing poorly determined eigenvectors with small eigenvalues; damping equivalently adds a small epsilon to the diagonal of the least-squares normal equations. Thus, we avoid making large changes to the model for negligible improvements in fitting the recorded data. Conjugate gradients converge first on the eigenvectors with the largest eigenvalues and with the largest contribution to the data.

This objective function is quadratic in each of the unknowns, but not in both simultaneously. A Gauss-Newton optimization will iteratively approximate this objective function by linearizing the forward modeling equation 6 in both unknowns.

Optimization requires the gradient of the objective function equation 7 with respect to each of the unknowns.

We can approximate a linear perturbation of the data $\delta d_j(t)$ with small perturbations of our model $\delta \hat{w}_{ij}(\tau)$ and $\delta r(t)$ as

$$\begin{aligned} \delta d_j(t) \approx & \int_{-\Delta\tau/2}^{\Delta\tau/2} \delta r(t-\tau) \sum_{i=1}^N \left[\hat{w}_{ij}(\tau) \cdot \cos\left(\frac{\pi\tau}{\Delta\tau}\right) \Lambda\left(\frac{t-i\Delta t}{\Delta t}\right) \right] d\tau \\ & + \int_{-\Delta\tau/2}^{\Delta\tau/2} r(t-\tau) \sum_{i=1}^N \left[\delta \hat{w}_{ij}(\tau) \cdot \cos\left(\frac{\pi\tau}{\Delta\tau}\right) \Lambda\left(\frac{t-i\Delta t}{\Delta t}\right) \right] d\tau \quad (8) \end{aligned}$$

The gradient of the objective function equation 7 with respect to the unknowns is just the transpose of this linearized operator on the data errors.

The gradient equation 9 with respect to the reflectivity is a correlation of each data error with the wavelets, then a sum over all traces

$$\begin{aligned} \frac{\partial J}{\partial r(t)} = & \sum_{j=1}^M \int_{-\Delta\tau/2}^{\Delta\tau/2} \left\{ [d_j(t+\tau) - d_j^R(t+\tau)] \right. \\ & \left. \cdot \sum_{i=1}^N \left[\hat{w}_{ij}(\tau) \times \cos\left(\frac{\pi\tau}{\Delta\tau}\right) \Lambda\left(\frac{t+\tau-i\Delta t}{\Delta t}\right) \right] \right\} d\tau + \epsilon_r r(t). \quad (9) \end{aligned}$$

The gradient (equation 10) with respect to the normalized wavelets is a correlation of the data error with the current reflectivity, with appropriate weighting for the windows and lags:

$$\begin{aligned} \frac{\partial J}{\partial \hat{w}_{ij}(\tau)} = & \int_0^T \left\{ [d_j(t) - d_j^R(t)] r(t-\tau) \cos\left(\frac{\pi\tau}{\Delta\tau}\right) \Lambda\left(\frac{t-i\Delta t}{\Delta t}\right) \right\} dt \\ & + \epsilon_w \hat{w}_{ij}(\tau). \quad (10) \end{aligned}$$

We now have all operations required for optimization with a Gauss-Newton optimization (Harlan, 2004). We can begin with wavelets that are impulsive and behave as an identity transform. Impulsive wavelets will result in a first estimate of reflectivity $r(t)$ that is the average of all data traces. A second iteration will adjust wavelets to better fit the average reflectivity, which will in turn improve the average reflectivity. Further iterations refine these results.

A Gauss-Newton optimization iteratively updates reference values for all unknowns and relinearizes the forward transform so that the objective function becomes purely quadratic in the perturbations (Luenberger, 1973). Linearized perturbations are then solved by least-squares conjugate gradients. Gauss-Newton finds an optimum

scale factor for linearized perturbations with a line search before adding them to reference values. Or, we can alternate updates of wavelets and reflectivities and avoid the line search (a modified Gauss-Seidel approach). Both approaches get to the same solution after a fairly small number of iterations (after adjusting the nonunique scale factor).

Even though reflectivity may be oversimplified, we are still able to estimate wavelets that describe very subtle changes in coherence and amplitude with offset. On the other hand, these wavelets cannot change rapidly over time and should find it difficult to fit changes unique to a single reflection, and not to its neighbors. This smooth consistency over time makes it more likely that wavelets describe residual transmission distortions and not changes in reflectivity (Harlan, 1989).

The estimated reflectivity can be used directly as a higher resolution least-squares stack of the data, with an implicit deconvolution of the estimated wavelets. If we want to remove the residual effects from our prestack data, then we can use these estimated wavelets explicitly to deconvolve the original data.

To deconvolve with our estimated wavelets, we return to our original modeling equation 1, which has a separate reflectivity $r_j(t)$ for each trace. We accept our wavelets $w_j(\tau, t)$ and data $d_j^R(t)$ as known and solve for each trace's reflectivity $r_j(t)$ with a purely linear least-squares inverse:

$$\min_{r_j(t)} \frac{1}{2} \sum_{j=1}^M \int_0^T \left[d_j^R(t) - \int_{-\Delta\tau/2}^{\Delta\tau/2} r_j(t-\tau) w_j(\tau, t) d\tau \right]^2 dt + \frac{\epsilon_r}{2} \int_0^T r_j(t)^2 dt. \quad (11)$$

This purely quadratic objective function can be iteratively optimized by conventional conjugate gradients. This deconvolution processes each trace $r_j(t)$ independently. There is no smoothing or mixing of amplitudes among traces.

As partial protection for AVO, the wavelets $w_j(\tau, t)$ can be normalized for unit rms amplitude before applying the deconvolution. This will still allow energy to be redistributed among frequencies, however. If the amplitude spectrum of each trace needs to be preserved, then wavelets can also be whitened without altering the phase (Claerbout, 1985).

Too much normalization will, however, prevent corrections of near-surface static filtering that is of no interest to AVO. It might be preferable instead to increase the interval among independent wavelets, which must then adapt more slowly over time and depth. Wavelets will then model residual corrections shared by a greater number of reflections.

EXAMPLES

In Figure 1a, we show a supergather from land data, sorted by increasing offset and combining several midpoint bins to increase fold. The data are sampled at 4 ms over time.

A crude NMO correction has been applied. RMOs are visibly not flat at farther offsets. An amplitude gain preserved some changes in amplitude with offset. Reflection wavelets change character, particularly in the strongest reflection around 3.8 s. Near-surface effects have damaged the continuity of central traces in many reflections. There is also some steeply dipping coherent noise that could have been removed first, but has been left in.

In Figure 1b, we show our final result, a deconvolution of the original data with some estimated dynamically changing wavelets. Notice the increased continuity and flatness of all reflectors.

Each wavelet was 51 samples (200 ms) long. The interval among independent wavelets was 300 samples (1.2 s). Reflectivities were assumed to have the same variance as the recorded data, and wavelets were given a variance of one. Noise was assumed to have 1000th of the variance of the data and reflectivity.

Reflectivities and wavelets were updated with six conjugate-gradient iterations each and four Gauss-Newton relinearizations. This amounts to 24 forward and transpose convolutions. The numerical cost is linear in the number of samples in a wavelet, but independent of the interval among wavelets.

The estimated dynamic wavelets themselves are visible in Figure 2a. To display, we began with

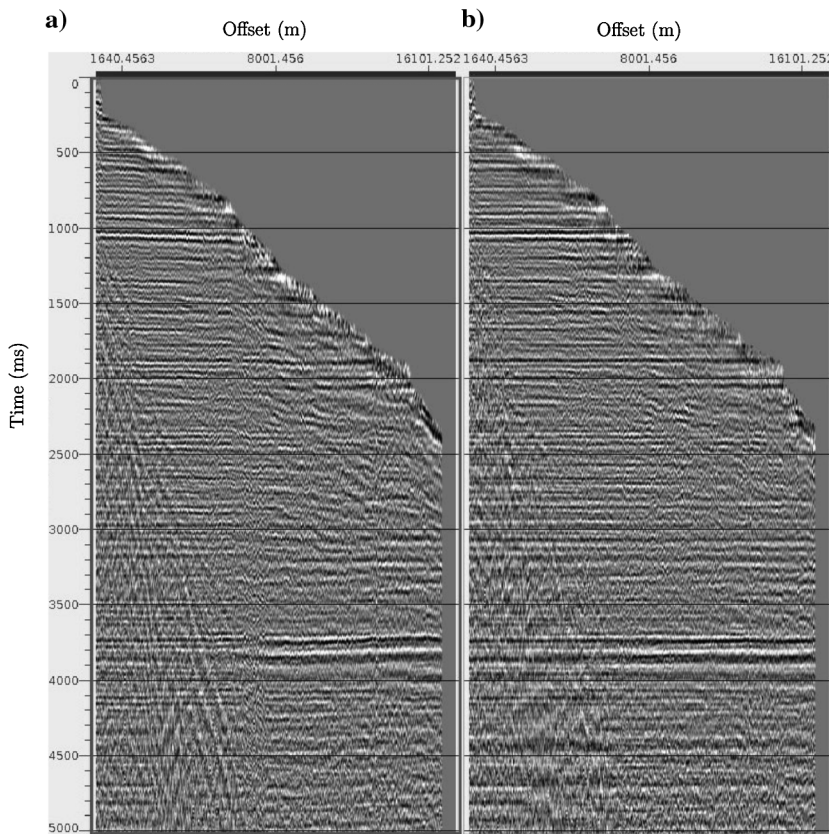


Figure 1. Prestack CDP supergather after (a) NMO correction and result after (b) wavelet balancing.

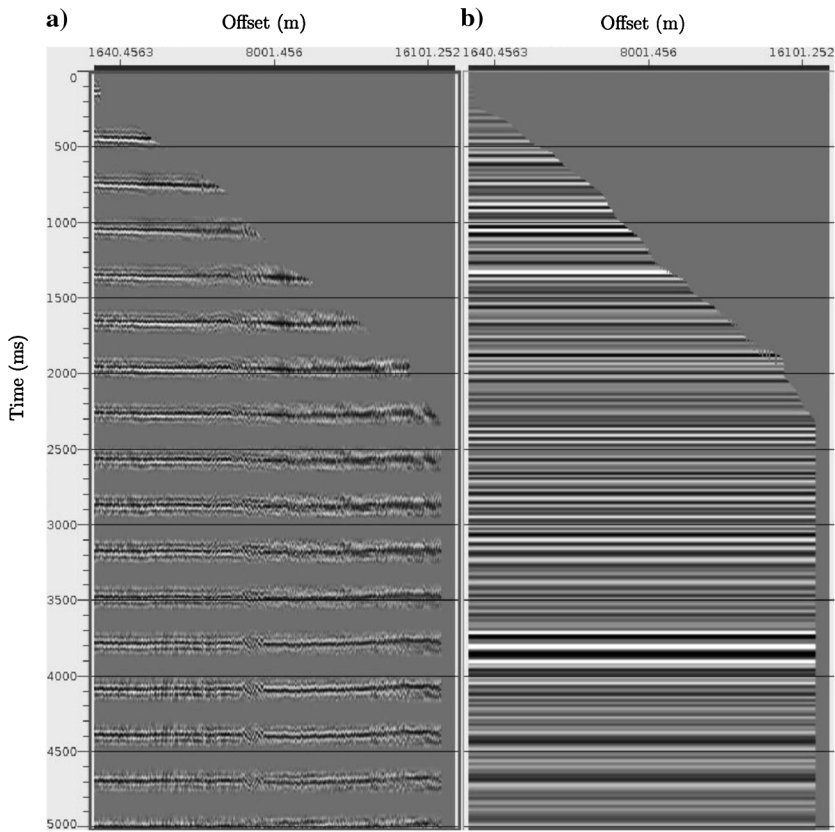


Figure 2. (a) Wavelets and (b) reflectivity. Wavelets can be convolved with the balanced result in Figure 1b to reconstruct the original data in Figure 1a.

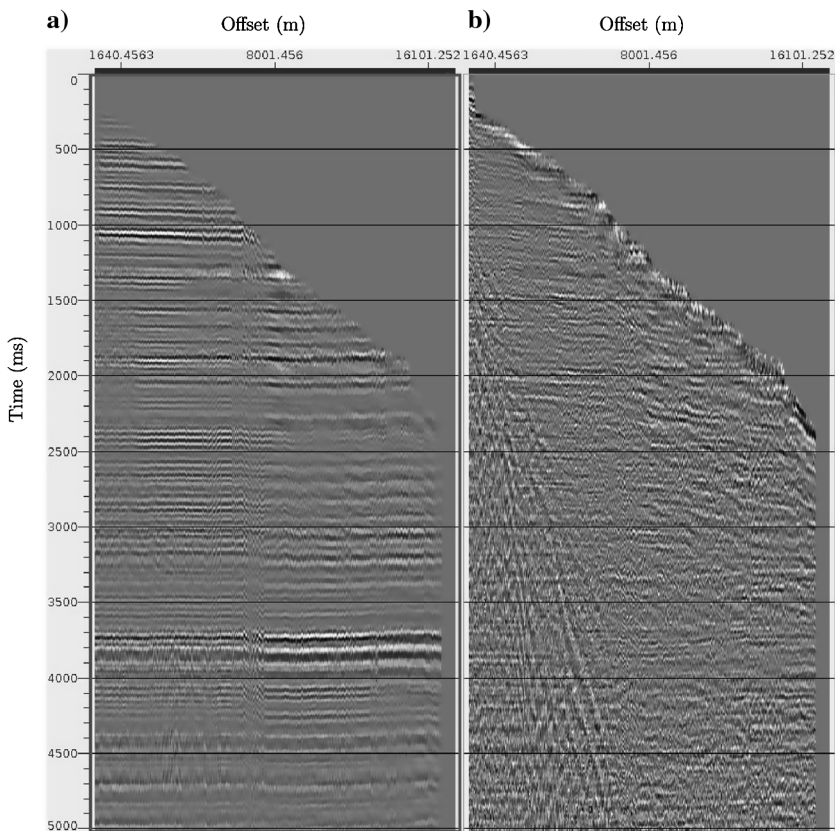


Figure 3. (a) The modeled data are a convolution of the wavelets and reflectivities in Figure 2. (b) The residual noise is the original data in Figure 1a minus the modeled data (a).

a reflectivity that contained impulsive spikes in every 101 samples (400 ms), then convolved with the dynamic wavelets. Changes over time are gradual because the interval among independent wavelets is 1.2 s.

Notice that wavelets show much more clearly the changes in coherence with offset and with time. RMOs are better determined because they must fit many adjacent reflections, no matter how weak. The static jumps in the central traces are very visible. Some steep coherent noise makes an imprint on inner offsets, but overall the effect is small. Wavelets were normalized to preserve the total squared amplitudes, but were not otherwise constrained.

Crosscorrelations or semblances should be able to detect the RMOs in these wavelets more easily than from the weak reflections in the original data. These wavelets average the residual coherence of multiple weak reflections and make it less necessary to choose isolated strong reflections. We can increase the signal-to-noise by

increasing the interval among independent wavelets, or we can increase resolution by decreasing the interval.

Figure 2b is the estimated reflectivity, which is the same for all traces, but with the original mute applied. This reflectivity can be substituted for a conventional stack.

In Figure 3a, we see the modeled data according to equation 4. This is a convolution of the wavelets and the reflectivities in Figure 2. Here, we can see how much of the variable coherence of these reflections can be explained with this simple convolutional model.

In Figure 3b, we see the unmodeled noise, the difference between the modeled data in Figure 3a and the original data in Figure 1a. Notice that the noise contains some dipping reflections, probably interbed multiples, that were too steep and variable to be modeled successfully by the wavelets, which is just as well. There are other flatter residual events near 2000 and 3700 ms. Some reflections may be neither constant in reflectivity nor modulate with offset in the

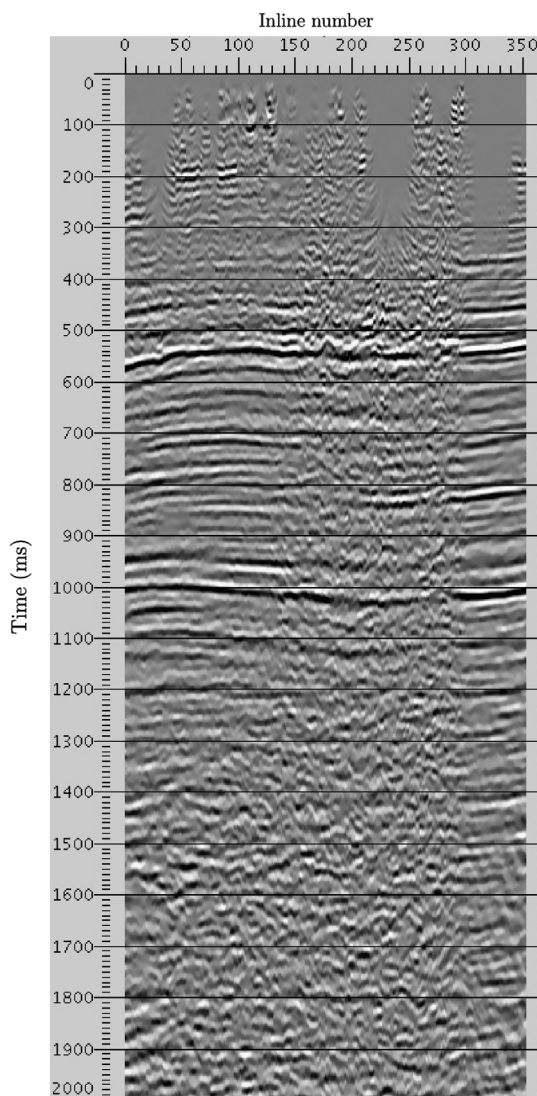


Figure 4. A section of stacked seismic data with structure to be processed like RMOs.

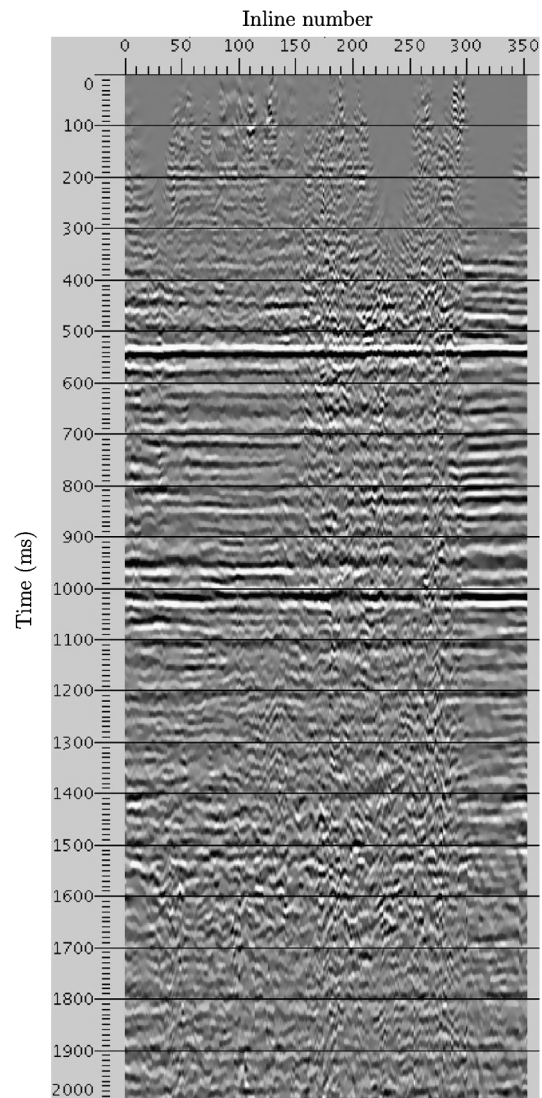


Figure 5. The same section after wavelet balancing, assuming flat reflectivity.

same way as nearby reflections. If so, we prefer that wavelets remain unable to model such AVO changes, which would be removed after deconvolution. We do not see any residual noise that appears entirely constant from near to far offset. Neither do we see any noise that appears consistently strong or weak at a single offset over a range of times (although this is harder to recognize).

Returning to the deconvolved data, Figure 1b, we see that lower frequencies in the steeply dipping dispersive noise become somewhat more coherent after deconvolution. Higher frequencies remained behind as steep noise in Figure 3b. Wavelets could not flatten much dipping noise without increasing misfits in flat reflections at the same frequencies.

As an additional stress test, we apply wavelet balancing to a segment of stacked seismic data in Figure 4. If we assume reflectivity should be flat, we can correct for structural changes as if

they were RMOs. The result appears in Figure 5. This workflow could be used for automatically tracking and picking horizons, but our main purpose is to test the robustness and convergence of the algorithm.

In Figure 6, we show the estimated wavelets, which can be convolved with Figure 5 to reconstruct the original data in Figure 4. This time, we used only normalized wavelets, without any cosine taper applied, to see the full range of lags. The estimated reflectivity shown in Figure 7 can be convolved with these wavelets for the modeled data in Figure 8. The noise in Figure 9 is the difference between the original and the modeled data.

Although this structure appears very arbitrary, it is still highly conformal and shows no visible faulting or other structural discontinuities. There are a few discontinuities that could be interpreted as residual static errors, particularly around inline number 300.

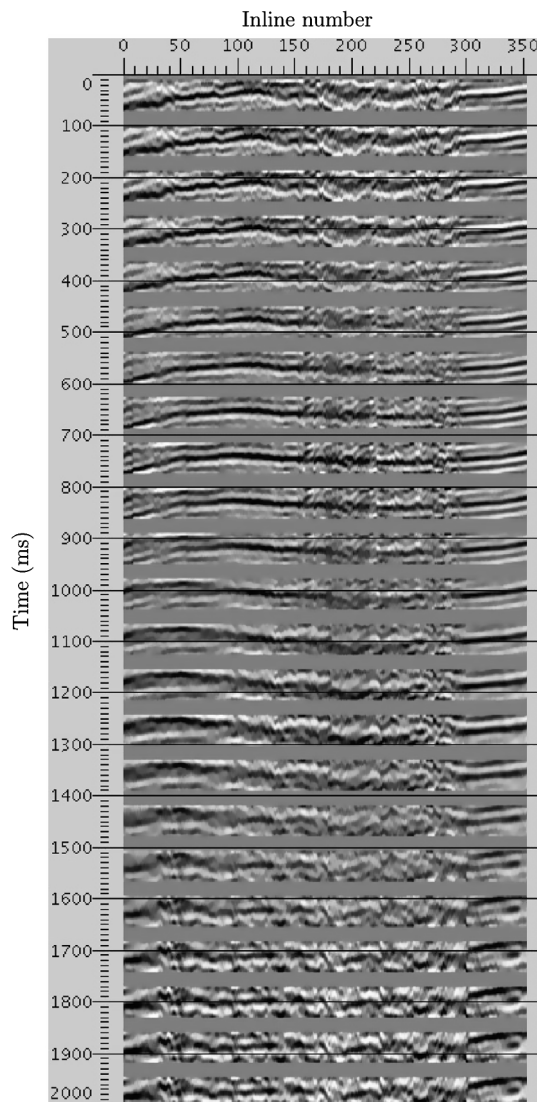


Figure 6. Estimated wavelets for the stacked data. No cosine taper has been applied.

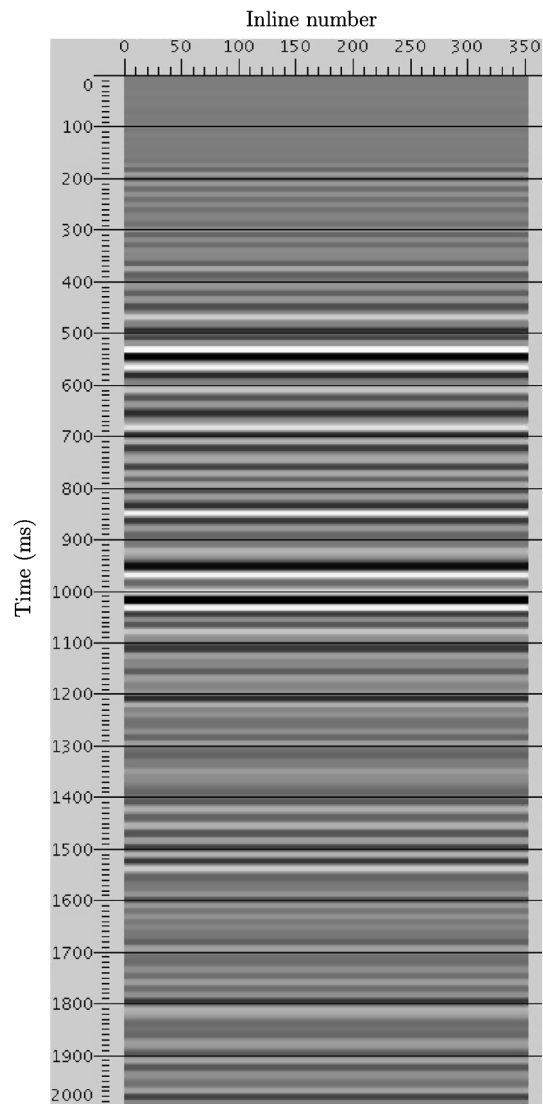


Figure 7. Estimated flat reflectivity.

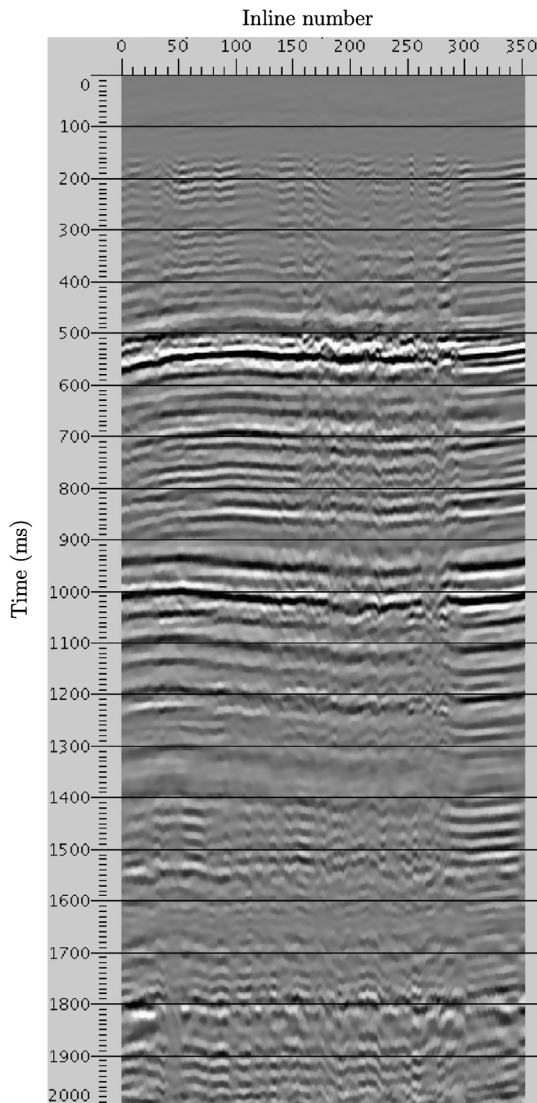


Figure 8. Reconstructed data that convolves reflectivity with wavelets.

Optimization is able to converge on a combination of wavelets and reflectivities that reproduce all these details very well. The deconvolution adjusts the structure by more than a wavelength, without any visible errors from cycle skipping. The strong reflector at 540 ms in Figure 5 appears much more continuous after wavelet balancing. After 1100 ms, we see little overall improvement in the lateral continuity of very incoherent reflections, including steeply dipping noise. This result shows a reluctance of the deconvolution to create coherent signal from completely random alignments of noise. The wavelets in Figure 6 show the structural coherence more clearly than the original noisy data. Even in the later noisier wavelets, we see clear structural trends, with shifts spanning the full width of the wavelets. The consistent coherence of wavelets is modeling reflections in Figure 8 that are weaker than the incoherent noise in Figure 9.

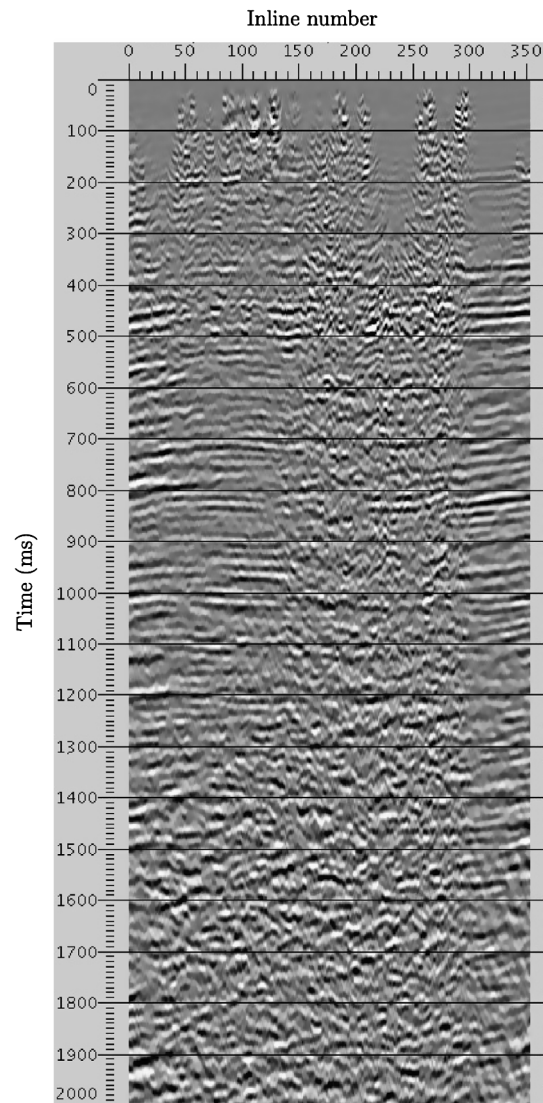


Figure 9. Noise after subtracting the reconstructed data from the original data.

CONCLUSIONS AND FUTURE DIRECTIONS

Estimated dynamic wavelets can capture the coherence of conventional RMO analysis, with additional frequency-dependent changes in phase shifts and amplitudes. Linearized optimization avoids the nonuniqueness and local minima of trace stretching.

For optimization, the most crucial parameters are the lengths of wavelets and the interval in time or depth among independent wavelets. In each case, we can adjust a trade-off between resolution and reliability, depending on the quality of our data. Longer wavelets allow for larger shifts in RMO. A shorter interval among wavelets allows moveouts to adapt more rapidly over time and depth. On the other hand, longer wavelets and shorter intervals increase the number of unknowns and reduce redundancy.

The most straightforward use of estimated wavelets is deconvolution of the original data. Deconvolution enhances the lateral continuity of traces, without any explicit mixing of amplitudes among traces.

Estimated wavelets could also take the place of the original data for semblance scans and crosscorrelations. These wavelets capture all residual coherence over a time interval shared by weak reflections that are individually difficult to pick.

We optimized reflectivities to fit as much coherence as possible before wavelets began to adjust residual coherence. A multiscale method could further adjust degrees of freedom in wavelets with each iteration, either reducing the interval among wavelets or increasing their lengths.

In examples, we normalized wavelets to preserve mean-squared amplitudes and to avoid nonuniqueness in scaling. These wavelets could also be whitened with zero-phase deconvolution to avoid redistributing amplitudes among frequencies. Phase shifts could be constrained to a narrower class of specific rotations.

The reflectivity model should include a smooth gradient with offset, reducing the need for wavelet normalization. Smooth variations in reflectivity could also account for vector offsets and Fresnel zones over 3D spatial midpoint directions.

Overall, we see much potential in replacing the stretch of conventional RMO with a model that explicitly distinguishes reflectivity from convolutional wavelets.

ACKNOWLEDGMENTS

The author thanks P. Cary for very helpful suggestions in his review of the manuscript.

REFERENCES

- Adler, F., and S. Brandwood, 1999, Robust estimation of dense 3D stacking velocities from automated picking: 69th Annual International Meeting, SEG, Expanded Abstracts, 1162–1165.
- Almomin, A., and B. Biondi, 2013, Tomographic full waveform inversion (TFWI) by successive linearizations and scale separations: 83rd Annual International Meeting, SEG, Expanded Abstracts, 1048–1052.
- Castagna, J., and M. Backus, eds., 1993, Offset-dependent reflectivity — Theory and practice of AVO analysis: SEG.
- Claerbout, J. F., 1985, Fundamentals of geophysical data processing: Pennwell Books.
- Cox, M., E. Scherrer, and R. Chen, 1999, Static corrections for seismic reflection surveys: SEG.
- Griffiths, L., F. Smolka, and L. Tremblay, 1977, Adaptive deconvolution: A new technique for processing time-varying seismic data: *Geophysics*, **42**, 742–759, doi: [10.1190/1.1440743](https://doi.org/10.1190/1.1440743).
- Hale, D., and S. Luo, 2013, Separating traveltimes and amplitudes in waveform inversion: 83rd Annual International Meeting, SEG, Expanded Abstracts, 969–974.
- Hale, D., and Y. Ma, 2013, Wave-equation reflection traveltime inversion with dynamic warping and hybrid waveform inversion: 83rd Annual International Meeting, SEG, Expanded Abstracts, 871–876.
- Harlan, W. S., 1989, Simultaneous velocity filtering of hyperbolic reflections and balancing of offset-dependent wavelets: *Geophysics*, **54**, 1455–1465, doi: [10.1190/1.1442609](https://doi.org/10.1190/1.1442609).
- Harlan, W. S., 1995, Regularization by model reparameterization. <http://billharlan.com/papers/regularization.pdf>, accessed 30 September 2014.
- Harlan, W. S., 2004, An implementation of generalized inversion. <http://www.billharlan.com/code/inv>, accessed 30 September 2014.
- Harlan, W. S., D. W. Hanson, and M. Boyd, 1991, Traveltime tomography and multioffset common-reflection points: 61st Annual International Meeting, SEG, Expanded Abstracts, 974–976.
- Hu, J., S. Fomel, and L. Ying, 2013, A fast algorithm for 3D azimuthally anisotropic velocity scan: 83rd Annual International Meeting, SEG, Expanded Abstracts, 4795–4799.
- Lazaratos, S., and C. Finn, 2004, Deterministic spectral balancing for high-fidelity AVO: 84th Annual International Meeting, SEG, Expanded Abstracts, 219–223.
- Lee, S., D. Hinkley, Y. Tang, and A. Baumstein, 2013, Tomographically enhanced full wavefield inversion: 83rd Annual International Meeting, SEG, Expanded Abstracts, 1037–1041.
- Levin, S., 1989, Surface-consistent deconvolution: *Geophysics*, **54**, 1123–1133, doi: [10.1190/1.1442747](https://doi.org/10.1190/1.1442747).
- Luenberger, D. G., 1973, Introduction to linear and nonlinear programming: Addison Wesley.
- MacKay, S., and R. Abma, 1993, Depth-focusing analysis using a wavefront-curvature criterion: *Geophysics*, **58**, 1148–1156, doi: [10.1190/1.1443498](https://doi.org/10.1190/1.1443498).
- Shuey, R., 1985, A simplification of the Zoeppritz equations: *Geophysics*, **50**, 609–614, doi: [10.1190/1.1441936](https://doi.org/10.1190/1.1441936).
- Stork, C., 1992, Reflection tomography in the postmigrated domain: *Geophysics*, **57**, 680–692, doi: [10.1190/1.1443282](https://doi.org/10.1190/1.1443282).
- Tsvankin, I., and V. Grechka, 2011, Seismology of azimuthally anisotropic media and seismic fracture characterization: SEG, Geophysical Reference Series 17.
- Ursenbach, C. P., and J. C. Bancroft, 2001, Playing with fire: Noise alignment in trim and residual statics: 71st Annual International Meeting, SEG, Expanded Abstracts, 1973–1976.